Radiation Physics and Chemistry 174 (2020) 108906

Contents lists available at ScienceDirect

Radiation Physics and Chemistry

journal homepage: www.elsevier.com/locate/radphyschem

Commercial filament testing for use in 3D printed phantoms

Matheus Savi[a,b,*], Marco A.B. Andrade[a], Maria P.A. Potiens[b]

[a] Federal Institute of Education, Science and Technology of Santa Catarina – IFSC, Av. Mauro Ramos, 950 – Centro, Florianópolis, Santa Catarina, 88020-300, Brazil
[b] Nuclear and Energy Research Institute – IPEN, Av. Prof. Lineu Prestes, 2242 - Butantã, São Paulo, SP, 05508-000, Brazil

ARTICLE INFO

Keywords:
3D printing
Phantoms
Computed tomography
Radiology

ABSTRACT

There is a great demand for phantoms by many areas of knowledge to be used for teaching or daily work. However, commercial phantoms are expensive and hard to obtain, especially in countries going through development. As an alternative, 3D printing can be the way to produce less expensive and reliable 3D phantoms. The goal of this study is to evaluate 14 available commercial filaments, in order to find if and how they can be used in 3D printed phantoms in computed tomography. Each material was printed as a 2 cm edge cube with rectilinear pattern and 60, 80 and 100% infill. The 80% infill of five other patterns were also printed and compared. Each 100% infill cube was weighted and had its density calculated. After that, the cubes were scanned in a Philips CT Brilliance 6 with 120 kVp, 200 mA, 2 mm slices and standard reconstruction. At the center of each cube, a ~120 mm^2 region of interest was set to measure the mean Hounsfield Unit (HU) and its standard deviation. The software *Origin* was used to plot HU results for rectilinear pattern, determine linear trends with its R^2 and compare achieved values with HU tissue range from literature. To confirm the response of HU values of selected tested materials in CT imaging as a function of percentage infill, a phantom prototype of a finger was 3D printed. The HU of the tested materials ranged from -516.2 ± 7.3 to 329.8 ± 18.9. All human tissues could be mimicked making use of these materials, except cortical bone above ~350 HU and tooth parts. The most promising filament was PLA + Cu, due to the multiple infill configuration that allows the resulting HU range to represent from adipose and skin tissue to marrow bone.

1. Introduction

There is a great demand for phantoms by many areas of knowledge such as medicine, dentistry, radiology, physics, medical physics, among others, ranging in uses from teaching material for classes to procedures in daily work. However, commercial phantoms are expensive and difficult to obtain, especially countries that are still in development, mainly due to the currency exchange rates, shipping and taxes. As an alternative, 3D printing might be the way to produce inexpensive and reliable phantoms that are aimed towards teaching and dosimetry.

Many technologies are available as of today for delivering the final manufactured product in form of a 3D printed object. The most common three types are: Polyjet/Multijet/Inkjet (*jet* technologies), Fused Filament Fabrication (FFF) or Fused Deposition Modeling (FDM – under trademark) and Stereolithography (SLA). The majority of papers published refers to Polyjet and FFF/FDM for construction and test of 3D printed phantoms and filaments as the type of choice (Filippou and Tsoumpas, 2018). Although Jet technologies are the most commonly used in 3D printing phantom construction as of 2018, with several materials already developed that fit in this practice, FFF technology is the most used worldwide, with 46%, while Jet tech, summed up, appears in third place with 37% of usage (Columbus, 2018; Sculpteo, 2018).

FFF printers, commonly known as desktop printers, were selected for this study due to low-cost acquisition of materials and machines. Regarding the materials, ABS (Acrylonitrile-butadiene-styrene) and PLA (Polylactic Acid) are found in most articles published. Some other materials were studied less frequently, such as Photoluminescent PLA,

* Corresponding author. Federal Institute of Education, Science and Technology of Santa Catarina – IFSC, Av. Mauro Ramos, 950 – Centro, Florianópolis, Santa Catarina, 88020-300, Brazil.
E-mail address: matheus.savi@ifsc.edu.br (M. Savi).

https://doi.org/10.1016/j.radphyschem.2020.108906
Received 16 July 2019; Received in revised form 29 March 2020; Accepted 1 April 2020
Available online 05 April 2020
0969-806X/

Table 1
Filaments used in this study.

Filament		Main substance	Additive (in mass)	Expected density[a] (g/cm^3)
ABS based	ABS	acrylonitrile butadiene styrene	–	1.01 to 1.09
	ABS+ (Premium)		–	NA
	WOOD		Wood (NA)	NA
PLA based	PLA	polylactic acid	–	1.22 to 1.30
	PLA + Bone		Cow bone (2%)	NA
	PLA + Al		Aluminum (25%–30%)	NA
	PLA + Brass		Brass (25%–30%)	NA
	PLA + Cu		Copper (25%–30%)	NA
	SILK		–	NA
Other plastic bases	HIPS	high impact polystyrene	–	1.03 to 1.16
	PETG	polyethylene terephthalate	Glycol	1.27 to 1.29
	PVA	polyvinyl alcohol	–	1.19 to 1.20
	TPU	thermoplastic polyurethane	–	1.05 to 1.21
	TPE	thermoplastic elastomer	–	0.86 to 1.26

[a] Information from datasheets or polymer databases(Kim et al., 2019; Polymerdatabse, 2019; UL, 2019).

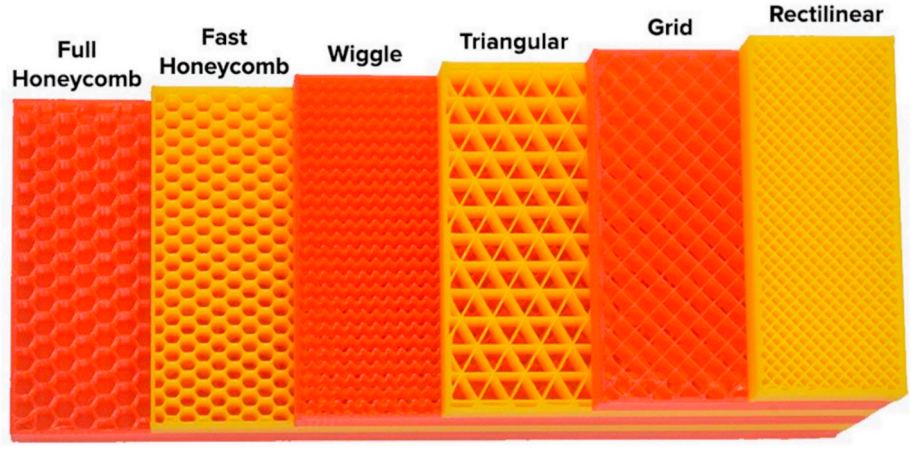

Fig. 1. Types of infill. Adapted from www.simplify3d.com.

PLA + Cu Woodfill, Bronzefill, Copperfill, PET, HIPS, TPU, TPE, PVA, Nylon and other filaments.

The goal of the study was to determine which and how the commercial filaments available in Brazil can be used, in 3D printing, in order to simulate human tissue in printed phantoms using computed tomography.

2. Materials and methods

Fourteen 3D printing filaments with 1.75 mm in diameter were tested in terms of their Hounsfield Unit (HU) using Computed Tomography (CT) scan and their density compared (see Table 1). Thirteen of them produced by UP3D are commercially available in Brazil, and one (PLA + Bone) produced by 3R3D was imported from Spain. The HU in CT is a map representation of linear attenuation (μ) of each material or tissue related to the linear attenuation of water, given as equation (1) (Hasieh, 2003).

$$HU = \frac{\mu_{material} - \mu_{water}}{\mu_{water}} x\ 1000 \quad (1)$$

Infill variation is one of the most common and important parameters that can be changed in every slicer software. Altering the percentage of filling and its shape, physical aspects of the printed model may be modified, especially density, which correlates directly to linear attenuation coefficient of photon radiation.

Each material (whose total cost for 12 kg of the aforementioned was

Table 2
HU ± SD for respective infill percentage and pattern per filament, at 120 kVp.

ABS based	Infill	%	ABS	ABS +	Wood
	RET	100	−133 ± 12	−57 ± 6	70 ± 6
		80	−306 ± 12	−213 ± 17	−82 ± 16
		60	−461 ± 11	−418 ± 8	−306 ± 8
	WIG	80	−338 ± 8	−239 ± 11	−164 ± 19
	FULL	80	−379 ± 14	−355 ± 17	−244 ± 10
	FAST	80	−357 ± 10	−327 ± 13	−219 ± 18
	GRID	80	−307 ± 13	−214 ± 7	−82 ± 12
	TRI	80	−276 ± 13	−199 ± 13	−42 ± 10

PLA based	Infill	%	PLA	PLA + Bone	PLA + Al
	RET	100	30 ± 13	35 ± 25	−72 ± 15
		80	−181 ± 10	−129 ± 29	−237 ± 12
		60	−370 ± 7	−344 ± 10	−336 ± 9
	WIG	80	−190 ± 8	−214 ± 51	−177 ± 4
	FULL	80	−304 ± 12	−275 ± 20	−323 ± 13
	FAST	80	−257 ± 10	−238 ± 17	−279 ± 9
	GRID	80	−130 ± 23	−139 ± 13	−209 ± 16
	TRI	80	−58 ± 19	−160 ± 33	−208 ± 16
	Infill	**%**	**PLA + Brass**	**PLA + Cu**	**SILK**
	RET	100	262 ± 14	330 ± 19	133 ± 8
		80	23 ± 18	49 ± 11	−23 ± 17
		60	−228 ± 8	−202 ± 13	−254 ± 16
	WIG	80	35 ± 19	94 ± 21	−59 ± 24
	FULL	80	−80 ± 12	−95 ± 22	−192 ± 16
	FAST	80	−27 ± 19	−36 ± 10	−147 ± 11
	GRID	80	26 ± 17	74 ± 13	−21 ± 31
	TRI	80	1 ± 15	103 ± 14	24 ± 19

Other plastics bases	Infill	%	HIPS	PETG	PVA
	RET	100	−109 ± 14	−25 ± 11	7 ± 14
		80	−312 ± 10	−229 ± 5	−178 ± 10
		60	−474 ± 9	−405 ± 5	−364 ± 9
	WIG	80	−285 ± 18	−256 ± 12	−172 ± 17
	FULL	80	−406 ± 13	−325 ± 7	−236 ± 11
	FAST	80	−397 ± 12	−321 ± 11	−207 ± 12
	GRID	80	−276 ± 12	−211 ± 7	−156 ± 17
	TRI	80	−291 ± 10	−211 ± 15	−132 ± 22
	Infill	**%**	**TPU**	**TPE**	
	RET	100	−37 ± 50	−235 ± 26	
		80	−268 ± 25	−370 ± 15	
		60	−360 ± 15	−516 ± 7	
	WIG	80	−177 ± 23	−388 ± 20	
	FULL	80	−289 ± 16	−502 ± 29	
	FAST	80	−322 ± 40	−452 ± 18	
	GRID	80	−247 ± 11	−402 ± 33	
	TRI	80	−270 ± 24	−420 ± 41	

of 730 USD) was printed, using Simplify 3D® slicer software (cost of 149 USD) and a FlashForge Creator Pro (cost of 650 USD) as printer, with a 2 cm edge cube with rectilinear pattern and 60, 80 and 100% infill. The 80% infill of five other patterns were printed in order to compare results with the standard rectilinear pattern. The shape of the infill patterns used in this study are shown in Fig. 1.

The weight of each cube with 100% infill was assessed as an arithmetic mean from three independent measurements on precision balance. The volumes of the same samples were assessed identically with liquid pycnometer in order to accurately calculate the solid volume of the samples, as differences in volume may occur between the planned and printed cubes. This technique is used to measure the volume of an irregular solid with known mass, through water displacement in a bottle. The previously known mass is divided by the volume of water displaced (equals its mass) and the density is, thus, determined (Hutten, 2016).

After that, the cubes were scanned in a Philips CT Brilliance 6 with 120 kVp, 200 mA, and the image volumes were acquired. This specific CT scanner passed by all quality assurance tests required by Brazilian regulations and went through warm up and air calibration in a daily basis to keep HU values accurate. From a DICOM image of 512 × 512 matrix, with 2 mm slices and standard reconstruction, at the center of each cube, an approximately 120 mm^2 region of interest (ROI) was set in order to measure the mean Hounsfield Unit and its standard deviation.

After ROI acquisition, the results were tabled and a graph expressing the HU value in terms of the infill percentage of the sample was plotted, in order to determine the linear fitting and its adjusted R^2 using Origin® software (OriginLab, USA). These calculations were made for the infill rectilinear pattern and the feasibility of use in 3D phantoms of each material which was studied, considering the HU range for some human tissues and organs in CT (Kalra, 2018).

To verify the method of infill percentage selection to achieve a desired HU value, a 3D printed phantom prototype of a human finger was constructed. To segment the finger CT from DICOM data, 3D Slicer (www.slicer.org) was used. For tissue mimicking based on the linear coefficients showed, Simplify 3D® (Simplify3D Inc, USA) was used to configure the 3D print phantom made in a FlashForge Creator Pro (Zhejiang Flashforge3d Technology Co., China).

3. Results and discussion

The values of Hounsfield Units found in this study are shown in Table 2. Comparison with and literature, considering works with same CT energy of 120 kVp and FFF printers are shown in Table 3. For ABS, the values correlate with some studies (Dancewicz et al., 2017; Okkalidis et al., 2018; Shin et al., 2017; Solc et al., 2018), for PLA, HIPS and TPU only one study correlates. For PLA + Cu, PETG, PVA and TPE, the values do not match.

A wide HU variation can be observed in literature, and there are some possible reasons for this difference to occur. The main one is because the materials derive from different manufacturers, who may possibly use different components, additives and colors in their fabrication, influencing directly in its properties. Other reason could be the fact that producers and sellers do not distinguish filament variations; for example, in ABS based filaments is difficult to know which filament its referred, ABS or ABS+. The same occurs for PLA that has two enhanced variations called PLA Premium (PLA+) and Advanced PLA (APLA). Another possible HU modifier can be the different CT equipments and/or CT scan parameters, with different physical and digital

Table 3
Comparison of HU ± SD for 100% infill at 120 kVp with literature.

Filaments		This Work	Okkalidis et al. (2018)	Dancewicz et al. (2017)	Shin et al. (2017)	Solc et al. (2018)
ABS based	ABS	−133 ± 12				−136 ± 35 −89 ± 25 101 ± 37
	ABS+	−57 ± 6	−66	−48[a]	−50 ± 13 −45 ± 13 7.3 ± 5	
PLA based	PLA	30 ± 13	136 20 –	119[a]	168 ± 16 173 ± 40 181. ± 6	−59 ± 19 81 ± 34 109 ± 18
	PLA + Cu	330 ± 19	120			
Other plastic bases	HIPS	−109 ± 14	−67		−55 ± 14	−56 ± 8 −103 ± 19 −118 ± 26
	PETG	−25 ± 11	−63		178 ± 6 165 ± 16	
	PVA	7 ± 14			229 ± 15	−52 ± 45 111 ± 8
	TPU	−37 ± 5			136 ± 27 100 ± 19	−53 ± 46
	TPE	−235 ± 26	21			

[a] Calculated with author data.

filters and algorithms used in acquisition, thus changing the final result of the same material.

Analyzing the HU from different infill patterns, it is possible to affirm that for nominal 80% infill, in comparison with the rectilinear pattern (RET), the Grid (GRID) and Triangular (TRI) ones have a potential to increase HU values, while Wiggle (WIG), Full Honeycomb (FULL) and Fast Honeycomb (FAST) patterns tend to decrease it, see Table 2.

Fig. 2 presents the dependence of HU values of tested filaments on percentage infill for the rectilinear pattern and compares them to HU values of the selected tissues. Parameters of linear fits of HU values, considering a the slope and the constant b to be used in equation (2), are presented in Table 4.

$$HU = a \times (infill\ \ \%) + b \tag{2}$$

This fitting was chosen because it was used before in attributive literature (Madamesila et al., 2016; Okkalidis et al., 2018) and had good results in the data with a high R^2 adjustment, besides allowing for better comparison with others and future studies. However, the linear trend should be interpreted carefully, as the extrapolation data came from 3 points ranging from medium to high infill. Theoretically, as the infill percentage diminishes, the amount of air inside the cube raises and proportionally the standard deviation, especially concerning values below 40%, which may turn the lower infill values into different ones from the intended.

Each of the aforementioned studied materials can mimic at least one human tissue in HU terms. The ABS and other plastic-based filaments studied are less suitable comparing to PLA, which demonstrates a higher versatility in tissue mimicking, with a good HU equivalence.

In terms of diagnostic radiology range 3D printed phantom construction capability, the ideal FFF printer filament must have the capability to make, in a single print, all kind of tissues, by varying only the infill percentage. This is extremely difficult, because making the structures separately may turn the phantom assembly impossible due to the anatomy variability with convex parts (a humerus passing through an arms muscles). Yet, air could be found between tissues made apart, as diaphragm and lung or due to the plastic contraction when cooled down. Other filaments physical characteristics as tissue linear attenuation equivalence and its response to other energy ranges (up to MeV) and Z_{eff} must be studied in the future. As it can be seen on Fig. 2, no filament studied here has the property of mimicking all tissues by only varying the infill. The best one found is the PLA + Cu, which may achieve −472 HU using 40% infill and 330 HU using 100% infill, corresponding to near lung parenchyma and low cortical bone densities, respectively.

Depending on the tissue, organ or anatomical structure desired to be 3D printed, a combination of filaments should be made by using a dual extruder printer or accessories, such as Mosaic Pallet® (Mosaic Manufacturing Ltd; Canada) multi material tool, to construct a more feasible 3D printed phantom. In both cases the filament must allow

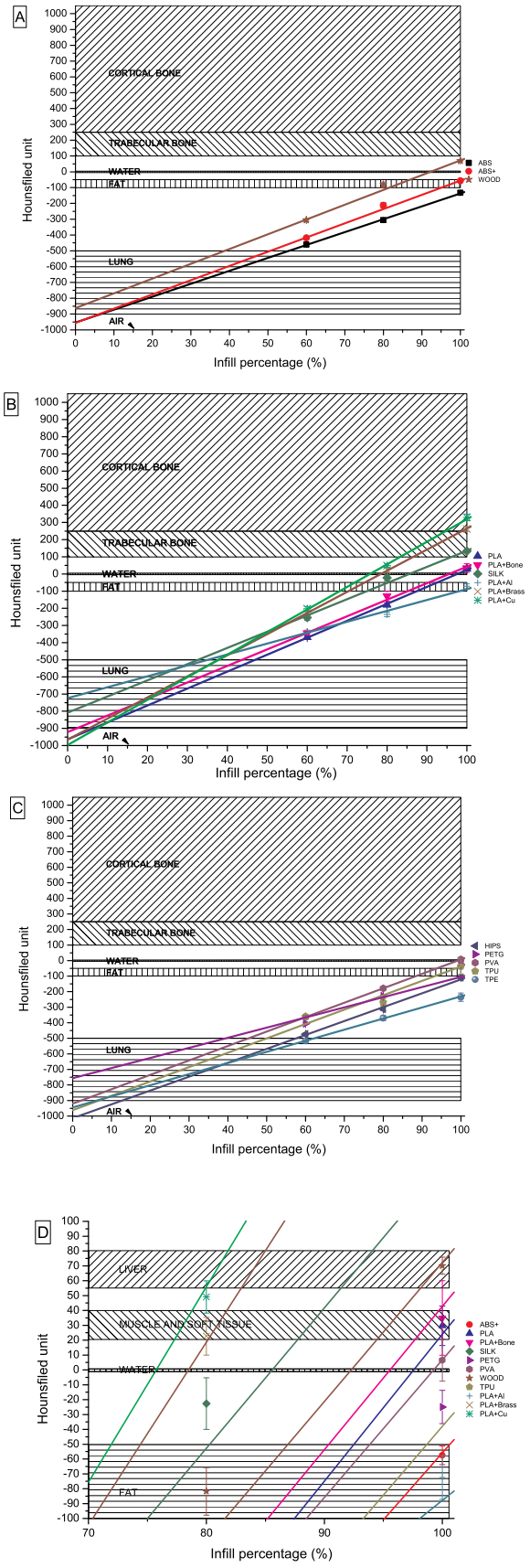

Fig. 2. Trends and tissues range in HU from (A) ABS based, (B) PLA based, (C) Other bases filaments and (D) Spot view of HU scale range.

adhesion between layers of different materials. For example, a combination of PLA + Cu and pure ABS may achieve an abdomen or thorax phantom; however, these two materials may not fuse correctly between layers.

3D printed phantom with the aim of acquisition protocols and image quality teaching in CT must consider that. According to previous study (Andrade et al., 2019), the value of 50% rectilinear infill should be the inferior infill limit, as the CT image became "gridded" when filled with air, containing perceptible spaces, decreasing its homogeneity.

The HU of the cortical bone ranges from 250 up to 1600 HU. Dentine and dental enamel only can be reproduced if the material achieves around 1600 HU and 2500 HU respectively.

It is desirable, but not excluding, that a material used to mimic the human tissue has its density equal or close to the one supposed to be reproduced (Xu and Eckerman, 2010). The density of the cubes with 100% infill differed from the predicted values presented in Table 1, by about 8% (ABS). That may occur in consequence of the printing parameters, although visually on CT image the infill of the cube appears full, gaps with air or contractions which happened after the plastic cooled down may interfere in the expected HU value, even on massive samples.

According to data of a previous study (Savi et al., 2017) the densities also respect a linear fitting with R^2 adjustment similar to the one of the presented HU. As result, the density values below the ones found in this study can be achieved in order to represent a specific human tissue.

Considering the theoretical data of density for organs and tissues published in ICRP 110 Annex A (ICRP, 2009), some of the materials with rectilinear pattern studied have the possibility of mimicking almost all tissues of the human body, with the exception of mineral ones such as bone, dentin and enamel. That is the case of all PLA based, except Al one, WOOD, PETG, PVA and TPU. This high level of compatibility happens since the majority of densities of the aforementioned described human tissues ranges from 1.02 to 1.05 g/cm^3. For skin (1.09 g/cm^3) and cartilage (1.1 g/cm^3), only PLA based ones are suitable, with the same exclusion of PLA + Al. Materials like ABS, ABS+ and PLA + Al, can mimic only a couple of tissues, like adipose breast and medullary tissue, as their density ranges from 0.950 to 0.980 g/cm^3. TPE is not suitable for mimicking human tissue at all.

Fig. 3 shows visualizations of each step in 3D printed phantom prototype construction. The first step was to segment and 3D preview a CT scan a hand, with 3D Slicer software (see Fig. 3A–D). Segmentation is the process of dividing the digital image in a set of pixels (Merjulah and Chandra, 2019).

In this case, two groups of pixels were set with HU range for soft tissue (green) and bone (yellow). After exporting from 3D Slicer, tissue and bone models in STL files were imported to Simplify 3D® (Fig. 3 E). The representation of software parameters setup used to 3D print the prototype can be seen in Fig. 3 J. Two regions of different infill were set using arbitrary 98% to bone (as PLA + Cu does not reach the mean measured HU value of 1200) and referenced, 76% for soft tissue (Fig. 3 I), using linear equation (2) with the coefficients found in Table 4.

Fig. 3(J) also shows the infill and attenuation relation, as the HU value of a ROI represents the mean of voxels, formed by a material with a determined (PLA + Cu) and air. When the amount of air increases in the model, the linear attenuation coefficient decreases. After the model printing, a 120 kVp and 200 mA CT scan with 2 mm slices reconstruction and standard algorithm was performed.

The CT image from the 3D printed finger phantom validates the method proposed to achieve a determined HU varying the infill percentage. This method can be used as a tool to create 3D printed phantoms in accurately way. This is noticeable especially for the soft

Table 4
Parameters of linear fits of HU values and density for rectilinear 100% infill for each filament.

Material		Linear coefficient		Adjusted R^2	Measured density (g/cm^3)
		a	b		
ABS based	ABS	8.19	−955	0.9990	0.9108 ± 0.0011
	ABS+	9.17	−951	0.9935	0.9919 ± 0.0007
	WOOD	9.40	−858	0.9879	1.0763 ± 0.0007
PLA based	PLA	9.98	−972	0.999	1.1027 ± 0.0080
	PLA + Bone	9.48	−905	0.9941	1.1312 ± 0.0455
	PLA + Al	6.60	−743	0.9805	0.9873 ± 0.0012
	PLA + Brass	12.27	−962	0.9998	1.1972 ± 0.0012
	PLA + Cu	13.29	−1005	0.9990	1.1273 ± 0.0018
	SILK	9.69	−824	0.9873	1.1837 ± 0.0008
Other plastic bases	HIPS	9.11	−1027	0.9957	0.9259 ± 0.0060
	PETG	9.50	−980	0.9982	1.0573 ± 0.0017
	PVA	9.26	−920	1.000	1.0504 ± 0.0032
	TPU	8.08	−868	0.9410	1.0795 ± 0.0029
	TPE	7.03	−936	0.9994	0.7940 ± 0.0091

tissue, as the HU value and its standard deviation matched the values found in the original CT used as base for segmentation, as shown in Fig. 3(I-J).

It is possible to identify a construction problem in the shell (3D printed parameter that modify solid external and internal coating just outside infill) to be solved in other studies. Shells are made of 100% material and creates a HU value which does not match with human body. That can be observed in the region supposed to mimic skin, as a high HU can be found, represented by a lighter color when compared to soft tissue.

4. Conclusions

This study made it possible to understand the response of HU values of selected tested materials with CT imaging as a function of percentage infill. It was possible to determine that HU is also susceptible to change in its values when different infill patterns were used, including raising the HU of a model.

The density of printed models of 100% infill is approximately 8% below expected value presented in Table 1, which indicates an issue in printing that needs to be studied in order to correct or diminish this difference. This study explores a small part of the several possible combinations of 3D printing parameters, which leads to a need for further studies on materials, infill percentage and infill patterns to improve tissue-equivalence of 3D printed phantoms.

Considering the results of this paper, many phantoms can be 3D printed with a significant tissue variation and accuracy using the FFF technique. The only three missing tissues were: high density cortical bones (above 800 HU), dentin and enamel, as the maximum HU value achieved was 350 HU for PLA + Cu.

New studies also must focus on the development of new filaments that are capable of mimicking a wide range of tissues, e.g. from lung to cortical bone, in order to allow 3D printing phantom construction in a single print, with one filament, while only varying the infill.

CRediT authorship contribution statement

Matheus Savi: Conceptualization, Methodology, Validation, Investigation, Resources, Writing - original draft, Project administration, Funding acquisition. **Marco A.B. Andrade:** Investigation, Resources, Writing - original draft, Writing - review & editing. **Maria P.A. Potiens:** Writing - review & editing, Supervision, Funding acquisition.

Declaration of competing interest

The authors declare that they have no known competing financial interests or personal relationships that could have appeared to influence the work reported in this paper.

The authors declare the following financial interests/personal relationships which may be considered as potential competing interests:

Matheus Brum marques Bianchi Savi.
Marco Antônio Bertoncini de Andrade.
Maria da Penha Albuquerque Potiens.

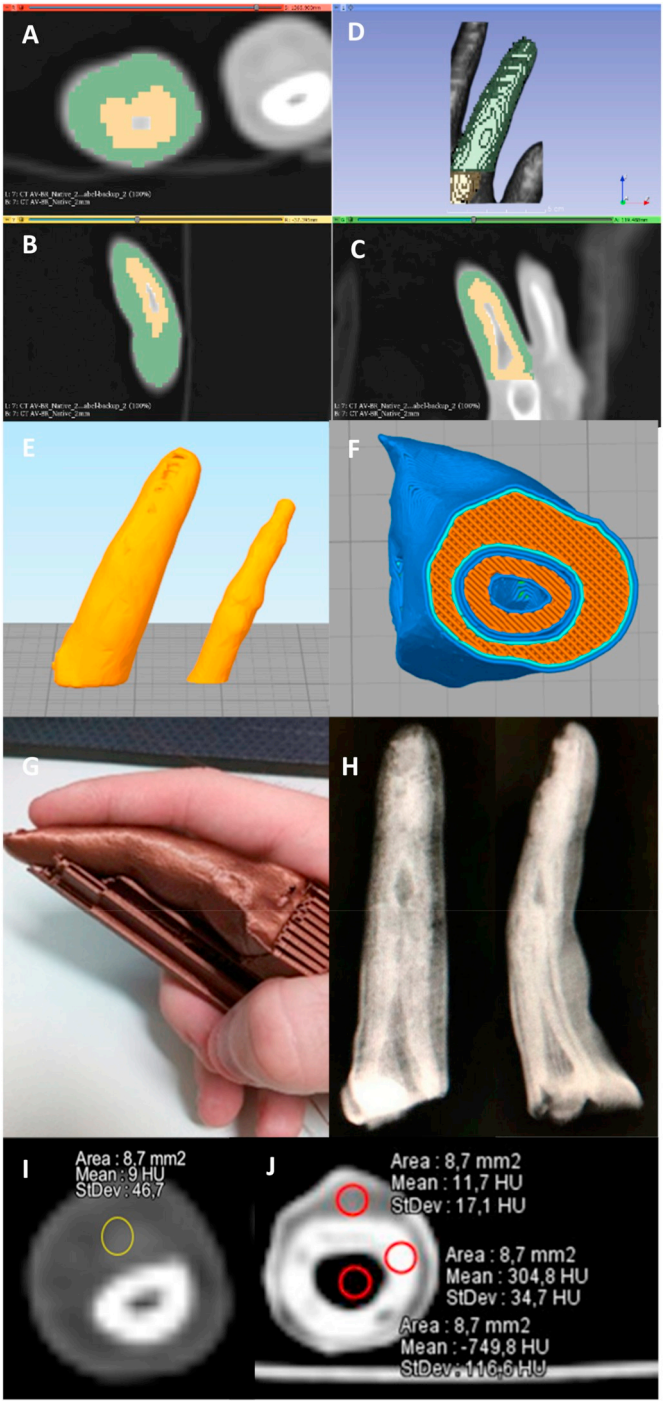

Fig. 3. A to C) Segmentation; D) 3D preview; E) 3D models; F) Printing Setup; G) Printed model; H) CT scout view; I) Axial slice with soft tissue ROI; J) Phantom axial slice with ROI measurement.

Acknowledgments

The authors would like to thank IFSC, IPEN, CAPES (Project 554/2018), FAPESP (PROJECT 2017/50332-0) and CNPq (PROJECT 312131/2016-0) for the partial financial support and the Children's Hospital Joana de Gusmão (Florianópolis/SC–Brazil) for the use of CT and X-ray equipment.

Appendix A. Supplementary data

Supplementary data to this article can be found online at https://doi.org/10.1016/j.radphyschem.2020.108906.

References

Andrade, M.A.B. de, Alves, C.O., Fin, A.P.C., Soares, F.A.P., Savi, M., Potiens, M..P.A. da, 2019. Visual impact of infill percentages for 3D printed radiologic simulators. In: International Joint Conference Radio 2019. São Paulo, pp. 5–7.

Columbus, L., 2018. The state of 3D printing, 2018 [WWW document]. accessed 11.28.19. https://www.forbes.com/sites/louiscolumbus/2018/05/30/the-state-of-3d-printing-2018/#23a54a807b0a.

Dancewicz, O.L., Sylvander, S.R., Markwell, T.S., Crowe, S.B., Trapp, J.V., 2017. Radiological properties of 3D printed materials in kilovoltage and megavoltage photon beams. Phys. Med. 38, 111–118. https://doi.org/10.1016/J.EJMP.2017.05.051.

Filippou, Valeria, Tsoumpas, Charalampos, 2018. Recent advances on the development of phantoms using 3D printing for imaging with CT, MRI, PET, SPECT, and ultrasound. Med. Phys. 45 (9), 740–760. https://doi.org/10.1002/mp.13058.

Hasieh, J., 2003. Computed Tomography: Principles, Design, Artifacts and Recent Advances, second ed. SPIE, Bellingham.

Hutten, I.M., 2016. Chapter 6 - testing of nonwoven filter media. In: Hutten, I.M. (Ed.), Handbook of Nonwoven Filter Media, second ed. Butterworth-Heinemann, Oxford, pp. 343–408. https://doi.org/10.1016/B978-0-08-098301-1.00006-X.

ICRP, 2009. ICRP 110: annexes A-D. Ann. ICRP 39, 47–70. https://doi.org/10.1016/j.icrp.2009.07.005.

Kalra, A., 2018. Developing FE human models from medical images. Basic Finite Elem. Method Appl. Inj. Biomech. 389–415. https://doi.org/10.1016/B978-0-12-809831-8.00009-X.

Kim, S., Chen, J., Cheng, T., Gindulyte, A., He, J., He, S., Li, Q., Shoemaker, B.A., Thiessen, P.A., Yu, B., Zaslavsky, L., Zhang, J., Bolton, E.E., 2019. PubChem 2019 update: improved access to chemical data. Nucleic Acids Res. 47, D1102–D1109. https://doi.org/10.1093/nar/gky1033.

Madamesila, J., McGeachy, P., Villarreal Barajas, J.E., Khan, R., 2016. Characterizing 3D printing in the fabrication of variable density phantoms for quality assurance of radiotherapy. Phys. Med. 32, 242–247.

Merjulah, R., Chandra, J., 2019. Chapter 10 - classification of myocardial ischemia in delayed contrast enhancement using machine learning. In: Hemanth, D.J., Gupta, D., Balas, V.E. (Eds.), Intelligent Data Analysis for Biomedical Applications, Intelligent Data-Centric Systems. Academic Press, pp. 209–235. https://doi.org/10.1016/B978-0-12-815553-0.00011-2.

Okkalidis, N., Chatzigeorgiou, C., Okkalides, D., 2018. Assessment of 11 available materials with custom three-dimensional-printing patterns for the simulation of muscle, fat, and lung Hounsfield units in patient-specific phantoms. J. Eng. Sci. Med. Diagnostics Ther. 1, 1–7. https://doi.org/10.1115/1.4038228.

Polymerdatabse, 2019. Poly(vinyl acetate) [WWW Document]. accessed 11.28.19. http://polymerdatabase.com/polymers/polyvinylacetate.html.

Savi, M., Potiens, M.P.A., Silveira, L.C., Cechinel, C.M., Soares, F.A.P., 2017. Density comparison of 3D printing materials and the human body. In: International Joint Conference Radio 2019, pp. 3–5.

Sculpteo, 2018. The state of 3D printing [WWW Document]. Ed. 2018. https://info.sculpteo.com/the-state-of-3d-printing-2018.

Shin, J., Sandhu, R.S., Shih, G., 2017. Imaging properties of 3D printed materials: multi-energy CT of filament polymers. J. Digit. Imag. 30, 572–575. https://doi.org/10.1007/s10278-017-9954-9.

Solc, J., Vrba, T., Burianova, L., 2018. Tissue-equivalence of 3D-printed plastics for medical phantoms in radiology. J. Instrum. 13https://doi.org/10.1088/1748-0221/13/09/P09018. P09018–P09018.

UL, 2019. Plastics prospector [WWW document]. accessed 11.28.19. https://plastics.ulprospector.com/.

Xu, X.G., Eckerman, K.F. (Eds.), 2010. Handbook of Anatomical Models for Radiation Dosimetry, first ed. CRC Press.